THE JOURNAL OF
PHYSICAL CHEMISTRY B

ARTICLE

pubs.acs.org/JPCB

Effect of the Substitution Pattern of Alkyl Side Chain in a Benzodithiophene Core π-System on Intra and Inter-Molecular Charge Carrier Mobility

Jun Kumagai, Koji Hirano, Tetsuya Satoh, Shu Seki,* and Masahiro Miura*

Department of Applied Chemistry, Faculty of Engineering, Osaka University, Suita, Osaka 565-0871, Japan

S *Supporting Information*

ABSTRACT: 3,7-Didocecyl-2,6-di(5-phenylthiophen-2-yl)benzo[1,2-*b*:3,4-*b*′]dithiophene (**1**) and its 4,8-didodecyl isomer **2** were prepared as the representative soluble X- and cross-shaped π-conjugated oligomer systems to provide insight into the effect of the substitution pattern of the alkyl side chain on electronic properties. The absorption and emission spectra as well as CV data showed the relatively longer effective conjugation of cross-shaped **2**. The intrinsic charge-carrier mobilities were then estimated by flash-photolysis time-resolved microwave conductivity (FP-TRMC) method and compared with their top contact FET properties. It was found that, although the TRMC method showed the higher mobility of **2** than **1**, the FET performance of **1** after appropriate conditioning and thermal annealing was superior to that of **2**. The effective conjugation of cross-shaped **2** is well reflected in the intramolecular mobility of positive holes estimated by FP-TRMC, showing striking contrast to the rather higher mobility of X-shaped **1** observed by FET as well as TOF measurements as the long-range translational motion of the carriers. This strongly suggests that the intermolecular packing of these compounds plays a significant role in the range of hole mobility of $<\sim 10^{-2}$ cm^2 V^{-1} s^{-1}.

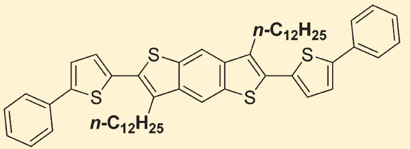

3,7-Dialkyl: ***X-Shaped***

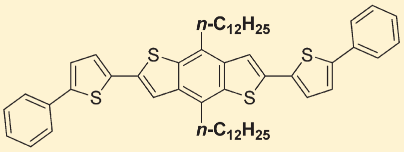

4,8-Dialkyl: ***Cross-Shaped***

■ INTRODUCTION

Poly- and oligoaryl compounds involving thiophene units have become increasingly important for the organic components of electronic devices including organic field effect transistors (OFETs), organic light-emitting diodes (OLEDs), and photovoltalic cells. Thus, their synthesis and properties of thiophene-fused aromatic compounds having benzothiophene and thienothiophene skeletons as well as oligothiophenes as the π-conjugated moieties have recently been studied extensively.[1] For solution-processable OFET components, rod- or ladder-like oligomers bearing two alkyl groups at their terminals, often the α-positions of thiophene units, are usually designed, whereas the β-alkyl derivatives are common for thiophene-based polymeric π-systems. In this context, it appears to be interesting to investigate the properties of β-alkyl derivatives of thiophene-based oligomers as partial models of the corresponding polymers.[2] Consequently, we have undertaken to prepare such types of compounds: [1,2-*b*:3,4-*b*′]benzodithiophene has been selected as the relatively rigid central core[3] and its 3,7-dialkylated and 2,6-di(5-phenylthiophen-2-yl)-capped derivative **1** has been prepared as a new, X-shaped oligomer (Figure 1). The 4,8-dialkyl isomer **2** as a cross-shaped derivative has also been synthesized.[4] Then, their fundamental properties have been investigated. For the estimation of their charge-carrier mobilities, flash-photolysis time-resolved microwave conductivity (FP-TRMC) method, which allows us to measure the intrinsic ability of a given sample, has been applied and compared with those measured by top contact FET.

■ RESULTS AND DISCUSSION

Our synthetic approaches to **1** and **2** are illustrated in Scheme 1. The benzo[1,2-*b*:3,4-*b*′]dithiophene core in **1** was constructed upon treatment of commercially available 1,4-phenylenediacrylic acid (**3**) with thionyl chloride in the presence of pyridine.[5] The resulting acid chloride **4** was transformed to the corresponding butyl ester **5** having substantial solubility. The subsequent Sonogashira coupling with 1-dodecyne using a catalyst system of $PdCl_2(PhCN)_2$/XPhos (XPhos = dicyclohexylphosphino-2′,4′,6′-triisopropylbiphenyl)[6] followed by hydrogenation in the presence of Pd/C enabled the introduction of dodecyl group to the 3- and 7-positions of the benzodithiophene motif. The removal of ester function was achieved by hydrolysis with aqueous KOH and Cu(0)-mediated decarboxylation to furnish the desired 3,7-didodecylbenzo[1,2-*b*:3,4-*b*′]dithiophene **9**. Finally, the regioselective dibromination with *N*-bromosuccinimide (NBS) and Stille coupling with tributyl(5-phenyl-2-thienyl)tin led to **1** in good yield. On the other hand, the preparation of **2**, a target for comparison, was readily accessible through the same cross-coupling strategy with the known compound **11**.[3] All of the new compounds were fully characterized by NMR and mass spectroscopy.

Received: April 19, 2011
Revised: May 25, 2011
Published: May 26, 2011

dx.doi.org/10.1021/jp2036668 | *J. Phys. Chem. B* 2011, 115, 8446–8452

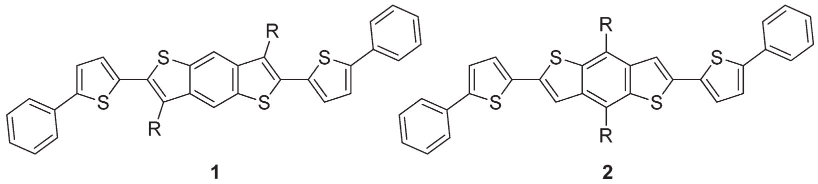

Figure 1. Structures of X- and cross-shaped oligomers, 3,7-didodecyl-2,6-di(5-phenylthiophen-2-yl)benzo[1,2-*b*:3,4-*b*′]dithiophene (**1**) and 4,8-didodecyl-2,6-di(5-phenylthiophen-2-yl)benzo[1,2-*b*:3,4-*b*′]dithiophene (**2**). *R* = *n*-$C_{12}H_{25}$.

Scheme 1. Synthetic Routes to Compounds 1 and 2

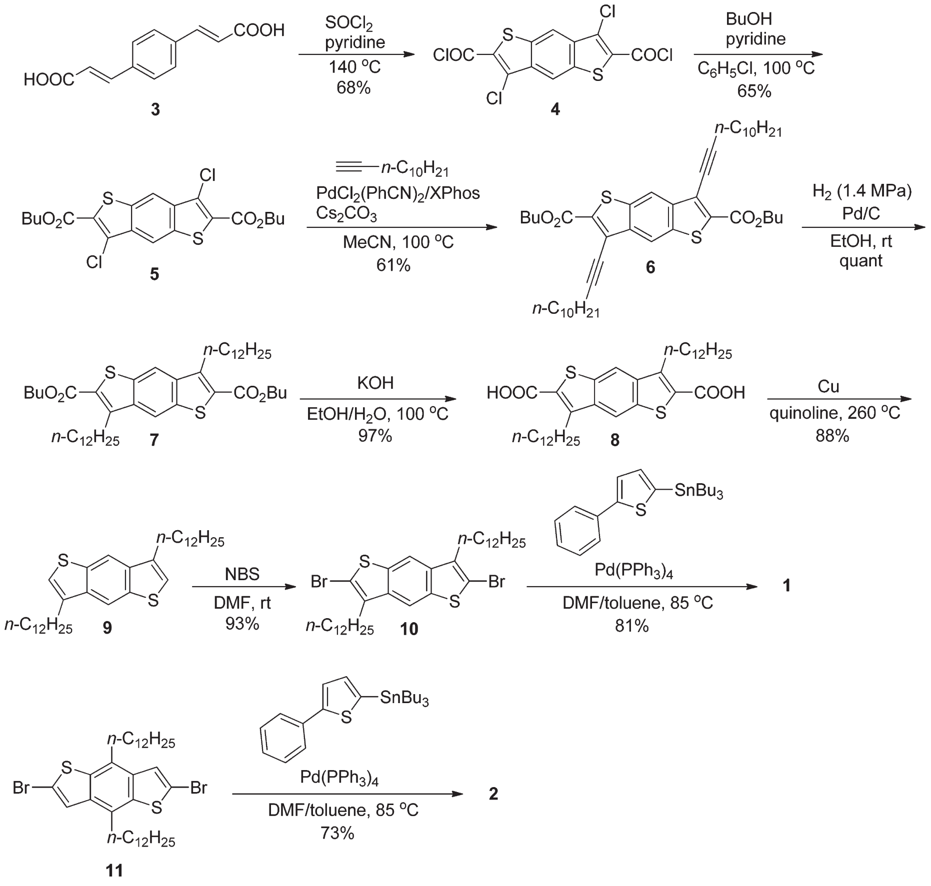

With the two desired oligomers in hand, we first investigated their optical properties in CH_2Cl_2 solutions (Figure 2 and Table 1). Although the absorption spectrum of X-shaped **1** exhibited the two major bands at λ_{abs} 296 and 390 nm, the emission one showed two bands centered at λ_{em} 456 and 484 nm. These peaks red-shifted in the cross-shaped oligomer **2**, which is indicative of relatively shorter effective conjugation length of **1**. On the contrary, the substitution pattern of the dodecyl group gave little influence on the absolute fluorescence quantum yield Φ. However, in the solid state, the Φ value of **1** was lower than that of **2** (Figure 3), suggesting the importance of substituent position for efficient self-assembly via intermolecular side-chain alignment.[7]

Cyclic voltammetric measurement of both **1** and **2** in CH_2Cl_2 solution displayed two reversible oxidation waves, in which **1** provided a 0.07 eV higher ionization potential than **2**, indicating a somewhat greater stability of **1** against oxidative doping (Figure 4 and Table 2). These observations were consistent with their absorption and emission spectra. It is worth noting that the outcome from the DFT calculations of their HOMO and LUMO levels using the ethyl models (*R* = Et for both **1** and **2**, see Figure 5) also paralleled the observed trends.

The optimized geometries of cross-shaped **1** and X-shaped **2** were also calculated by DFT method with B3LYP/6-31G(d) basis sets using Gaussian 03 code.[8] Unlike the complete planner structures of compound **2** in steady state, compound **1** shows apparently the twisted structures at both the ends of the molecule. The symmetrical lobes of HOMO are observed on the end-phenyl rings in compound **2**, suggesting the effective mixing of π-orbitals in the phenyl rings to the HOMO of the compound. This may be the case given the slightly lower HOMO level relative to that in compound **2**.

The thermal properties of **1** and **2** were also investigated by differential scanning calorimetry (DSC) with the temperature range of −20 to +200 °C at a rate of 2 °C min^{-1} (Figure 6).

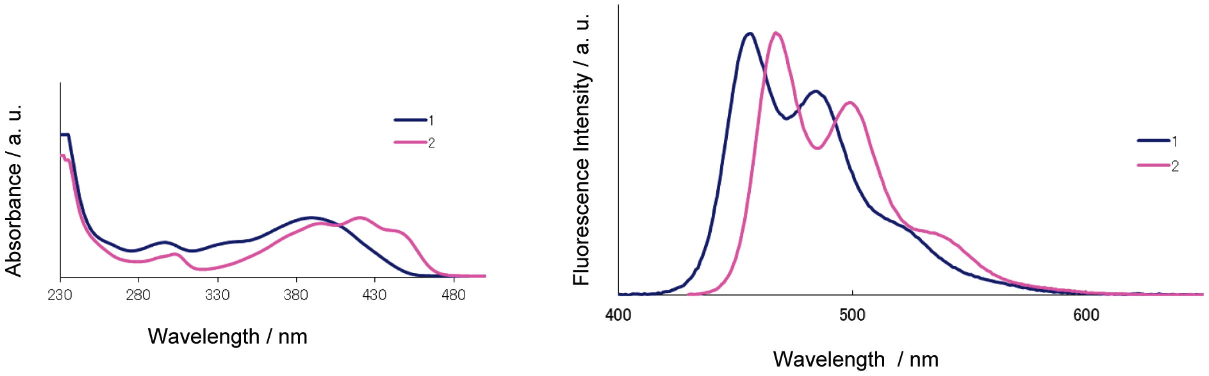

Figure 2. Absorption (left) and emission spectra (right) of compounds **1** and **2** in CH_2Cl_2 solution.

Table 1. Photophysical Data of Compounds 1 and 2 in CH_2Cl_2 Solution

compd	λ_{abs} (nm)[a]	λ_{em} (nm)[b]	E_g (eV)[c]	log ε	Φ[d]
1	296/390	456/484	2.8	4.6	0.63
2	303/396/420	468/499	2.7	4.5	0.58

[a] Absorption maximum in CH_2Cl_2 (5.0×10^{-6} M). [b] Emission maximum in CH_2Cl_2 (5.0×10^{-6} M). [c] Optical band gap. [d] Absolute fluorescence quantum yield.

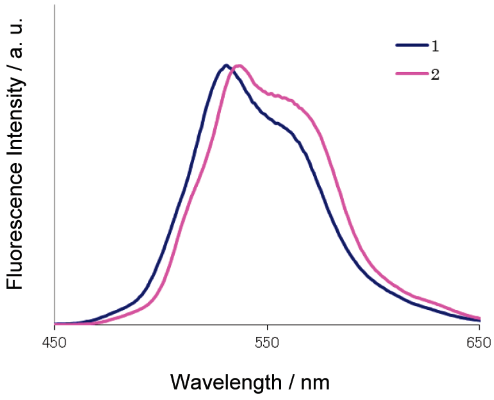

Figure 3. Emission spectra of compounds **1** and **2** in solid state: **1**: λ_{em} 531 nm, Φ = 0.20; **2**: λ_{em} 537 nm, Φ = 0.36.

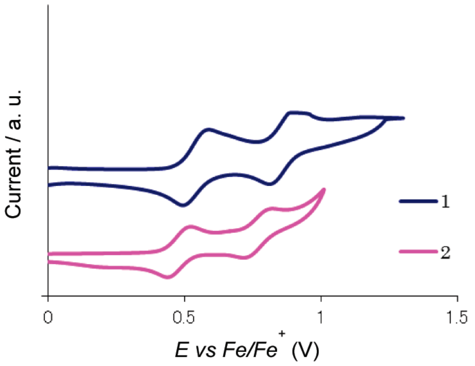

Figure 4. Cyclic voltammograms of **1** and **2** in CH_2Cl_2 containing 0.1 M Bu_4NPF_6 at a scan rate of 100 m V s^{-1}.

Table 2. Cyclic Voltammogram Data and Optical Properties of 1 and 2[a]

compd	$E_{ox}^{1/2}$ (V)[a]	E_{HOMO} (eV)[b]	E_{LUMO} (eV)[c]	E_g (eV)[d]
1	0.55/0.84	−5.35 (−5.00)[e]	−2.55 (−1.88)[e]	2.8
2	0.48/0.77	−5.28 (−4.90)[e]	−2.58 (−1.96)[e]	2.7

[a] Performed in Bu_4NPF_6/CH_2Cl_2 solution. ν = 100 mV/s, versus Fe/Fe^+. [b] HOMO = $-4.8 - E_{ox}^{1/2}$. [c] Estimated from HOMO, E_g: $E_{LUMO} = E_{HOMO} + E_g$. [d] Optical band gap. [e] Calculated by B3LYP/6-31G(d) using the ethyl models (*R* = Et for both **1** and **2**).

The phase transitions of **1** and **2** appeared at 99 and 157 °C, respectively.

The higher transition temperature associated with the larger enthalpy change ($\Delta H \sim$ 3-hold in cross-shaped **2** relative to X-shaped **1**) is due to the effective π-stacking in the solid state of cross-shaped **2**, and this is also supported by the presumed planner structure in cross-shaped **2** leading to the dense molecular packing.

Prior to the investigation of the FET performance of **1** and **2**, the measurement by time-resolved microwave conductivity (TRMC) method[9,10] was carried out for the estimation of their intrinsic charge mobility (Figure 7 and Table 3). The intrinsic mobility $\Sigma\mu$ of X-shaped **1** was calculated to be 1.6×10^{-2} cm^2 V^{-1} s^{-1}, whereas that of cross-shaped **2** showed a higher value of 4.8×10^{-2} cm^2 V^{-1} s^{-1}. This suggests that the local motion of charge carriers in these compounds is in the same order with each other.

In the range of excitation photon density, cross-shaped **1** shows negligible dependence of the observed maximum values of conductivity as shown in Figure 7a. However, the values decrease considerably in X-shaped **2**, as plotted in Figure 7c. The higher values of mobility in X-shaped **2** are responsible for the contribution from second-order bulk recombination reactions in the crystalline domains, whereas pseudo first-order recombination kinetics is observed in Figure 7a for **1**. Thus the second-order bulk recombination analysis was performed for the transient conductivity of X-shaped **2** as shown in Figure 7d, giving a clear contribution from the recombination processes between positive and negative charges.[11]

The major charge carrier species in the compounds were also determined by time-of-flight (TOF) measurements. The current transients were observed only under the positive bias mode (positive bias applied at top electrodes), suggesting strongly holes as the major charge carriers. Based on the TOF measurement, the estimated yields of photocarrier generation upon excitation at 355 nm are also listed in Table 3.

The observed pseudosecond order rate constants in the TRMC transients are increasing linearly from 0.055 to 0.11 μs^{-1} upon

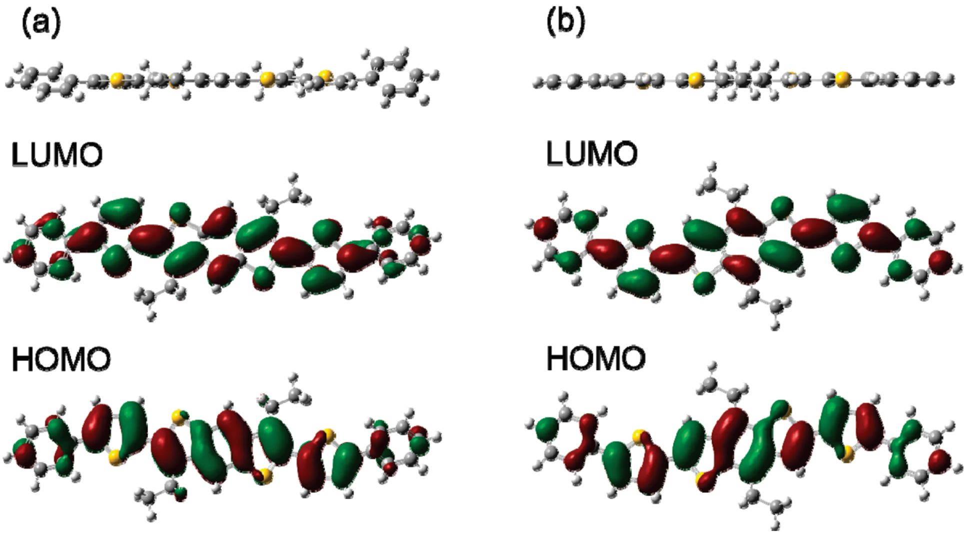

Figure 5. Optimized geometries of compounds (a) **1** and (b) **2** calculated by DFT method with B3LYP/6-31G(d). Molecular orbitals calculated at HOMO and LUMO levels are also presented for the respective compounds **1** and **2**.

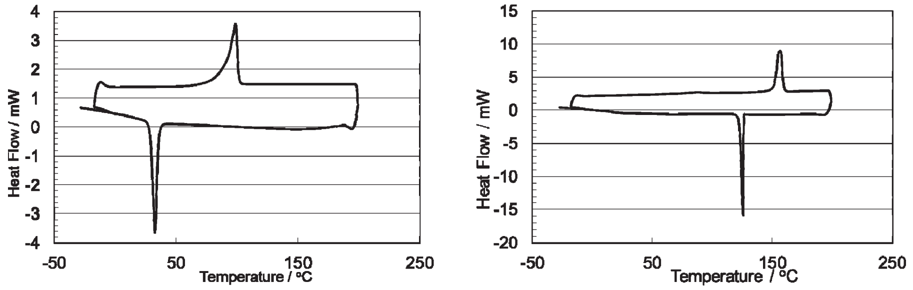

Figure 6. DSC thermograms of **1** (left) and **2** (right).

excitation photon density ranging from 5.2×10^{14} to 7.5×10^{16} photons cm^{-2}. On the assumption of the diffusion controlled bulk recombination reactions as 10^{10} mol^{-1} dm^3 s^{-1}, the predicted concentration of negative and positive charge carriers are ~100 nmol dm^{-3} within 1 μs after the pulse exposure. In contrast, the absorption coefficient of the solid state X-shaped **2** is 1.5 μm^{-1} at 355 nm (based on the $\varepsilon = 1.2 \times 10^4$ mol^{-1} dm^3 cm^{-1} at 355 nm, and the density of $\rho \sim 1$ gcm^{-3}), leading to the averaged initial charge carrier density of 20 to 2.9×10^3 nmol dm^{-3} under the excitation photon density range with $\varphi = 6.2 \times 10^{-3}$. This shows good agreement with the concentration in the second-order recombination analysis, suggesting strongly the adequacy of using φ values estimated by TOF measurements for the mobility derived from TRMC analysis.

Figure 7e shows the values of mobility determined by the TOF measurement as a long-range translational motion of holes in these compounds. Cross-shaped **1** showed 1 order of magnitude higher value of mobility than that of X-shaped **2**. The small slopes of the electric field dependence, especially in X-shaped **2**, suggest strongly the presence of the large hopping barriers in the media.[12] Thus the following FET device fabrications were tested under varying surface structures and annealing conditions.

The top contact FET devices based on both **1** and **2** exhibited typical p-type FET responses. The parameters extracted from transfer characteristics are listed in Table 4. With neither surface treatment nor annealing, the device based on cross-shaped **2** gave a higher mobility than that with **1** (entries 1 and 4), consistent with the preliminary investigation by the TRMC method. In contrast, the surface modification of SiO_2 with ODTS (octadecyltrichlorosilane) and an appropriate annealing to achieve higher structural orders dramatically improved the FET performance of **1** (entry 2). Since the attempt on ODTS modification for **2** was failure due to difficulties in the deposition step, the annealing alone was carried out (entry 5). However, the positive effect was quite small, and its mobility was sluggishly improved. The best performance was obtained when the device based on **1** was prepared with a longer source/drain pair was used (entry 3): its mobility (μ), on/off current (I_{on}/I_{off}), and threshold voltage (V_{th}) were 3×10^{-3} cm^2 V^{-1} s^{-1}, 10^{-4}, and −36 V, respectively. The transfer characteristics and output curves at different gate voltages of some **1**- and **2**-based FET devices are shown in Figure 8.[13]

CONCLUSION

We have synthesized 3,7-didocecyl-2,6-di(5-phenylthiophen-2-yl)benzo[1,2-*b*:3,4-*b*′]dithiophene (**1**) and its 4,8-didodecyl isomer **2** as the representative soluble X- and cross-shaped oligomers bearing a benzodithiophene central core and compared their hole mobilities as well as optical and thermal properties. Although the FP-TRMC method indicates the higher charge-carrier mobility of **2**, the **1**-based device after appropriate surface treatment and annealing proved to be superior to the

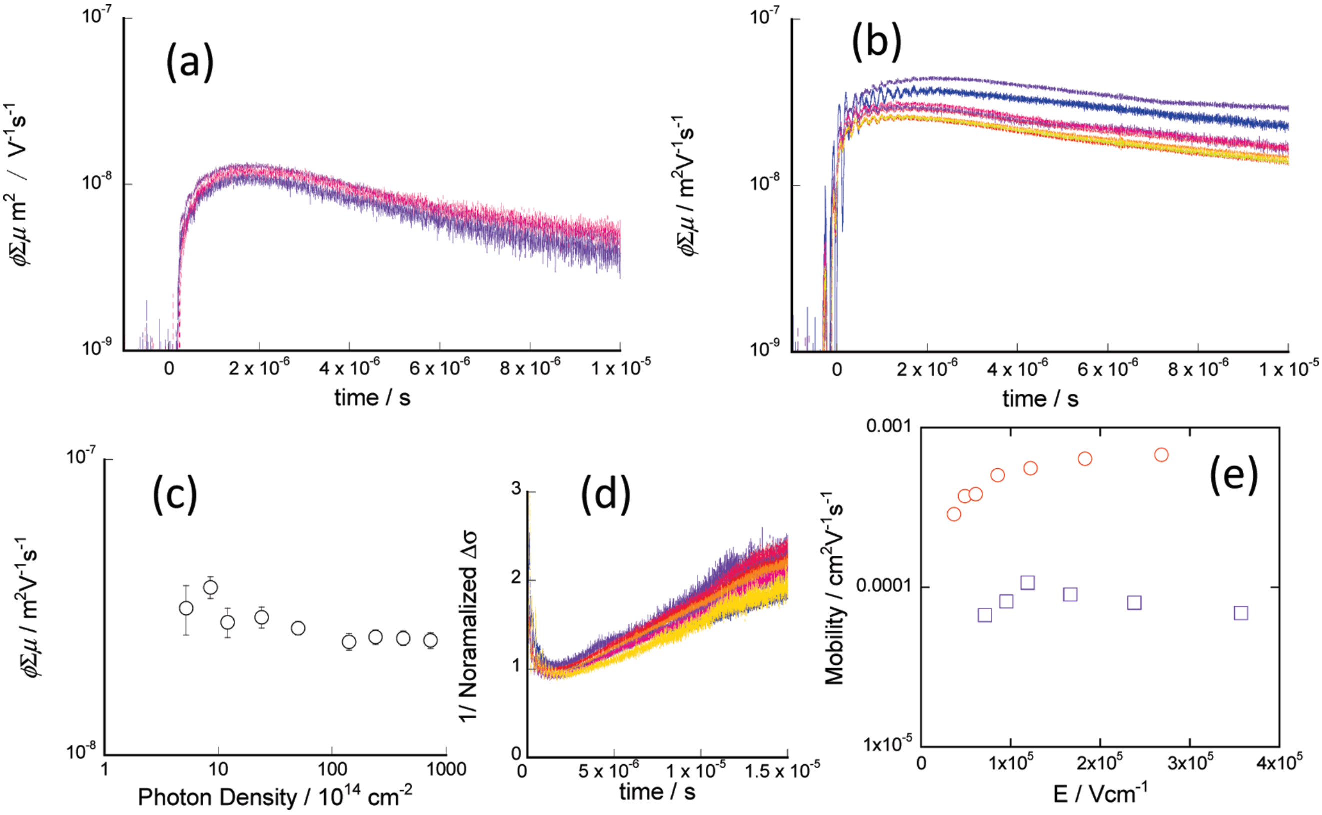

Figure 7. Microwave conductivity transients of **1** (a) and **2** (b) upon 355 nm irradiation at excitation photon densities of (a) $2.1 \times 10^{15} - 2.8 \times 10^{16}$ and (b) $5.2 \times 10^{14} - 7.5 \times 10^{16}$ photons cm^{-2}, respectively. Observed maximum values of the transient conductivity of compound **2** were plotted vs excitation photon density in panel c. (d) The second-order recombination analysis of the conductivity transient observed for compound **2** in the range of excitation photon density. (e) The dependence of hole drift mobility determined by time-of-flight measurements on the applied electric field strength at 273 K. Circles and squares are the mobility observed in compounds **1** and **2**, respectively.

Table 3. Results of Measurement by TRMC and TOF Methods

compd	$\varphi_{max}\Sigma\mu$ (cm^2 V^{-1} s^{-1})	φ_{max}[a]	$\Sigma\mu$ (cm^2 V^{-1} s^{-1})	μ_+ (cm^2 V^{-1} s^{-1})
1	1.3×10^{-4}	8.1×10^{-3}	1.6×10^{-2}	7×10^{-4}, [b]
2	3.0×10^{-4}	6.2×10^{-3}	4.8×10^{-2}	9×10^{-5}, [b]

[a] Estimated by time-of-flight (TOF) method. [b] Hole drift mobility determined by TOF measurement at 5.2×10^5 V cm^{-1} (compd **1**) and 1.6×10^5 V cm^{-1} (compd **2**), respectively.

Table 4. FET Performances of 1 and 2

entry[a]	compd	surface treatment	annealing	μ (cm^2 V^{-1} s^{-1})	I_{on}/I_{off}	V_{th} (V)
1	**1**	bare	none	3.0×10^{-5}	10^3	-40
2	**1**	ODTS	60 °C for 30 min	1.0×10^{-3}	10^4	-33
3[b]	**1**	ODTS	60 °C for 30 min	3.0×10^{-3}	10^4	-36
4	**2**	bare	none	2.0×10^{-4}	10^3	-35
5	**2**	bare	60 °C for 30 min	3.0×10^{-4}	10^3	-35

[a] Channel width (W) and length (L): $W \times L = 2000\ \mu$m $\times$ 20 μm. [b] $W \times L = 2000\ \mu$m $\times$ 50 μm.

2-based one. These results provide intriguing insight into the substitution pattern of alkyl side chain on the intra- and intermolecular charge carrier mobility. Further application of the X-shaped core to other π-conjugated poly- and oligothiophene derivatives are now in progress.

■ EXPERIMENTAL SECTION

Instrumentation and Chemicals. ^{1}H and ^{13}C NMR spectra were recorded at 400 and 100 MHz for CDCl$_3$ or DMSO-d_6 solutions, respectively. MS data were obtained by EI or FAB. Silica gel (Wakogel 200 mesh) was used for column chromatography. Abosorption and photoluminescence spectra were measured as described previously.[14] Cyclic voltammetry (CV) was carried out on a BAS CV-50W voltammetric analyzer at a scan rate of 100 mV s^{-1} in CH$_2$Cl$_2$ containing 0.1 M Bu$_4$NPF$_6$ as supporting electrolyte, using a platinum button as the working electrode, a platinum wire as the counter electrode, and Fe/Fe$^+$ (ferrocene/ferrocenium) as the reference redox couple. Differential scanning calorimetry (DSC) measurements were performed on a 2920 MDSC V2.6A. The TRMC measurements were implemented by Nd:YAG laser (third harmonic generation THG (355 nm) from Spectra Physics INDY-HG (fwhm 5−8 ns)).[9] The FET devices were characterized with a Keithley 4200 probe station under reduced pressure. X-ray diffraction (XRD) patterns were obtained by using Rigaku RINT 2000.

Unless otherwise noted, materials obtained from commercial suppliers were used without further purification. Dicyclohexylphosphino-2′,4′,6′-triisopropylbiphenyl (XPhos) was purchased from Aldrich. Tetrakis(triphenylphosphine)palladium (Pd(PPh$_3$)$_4$)

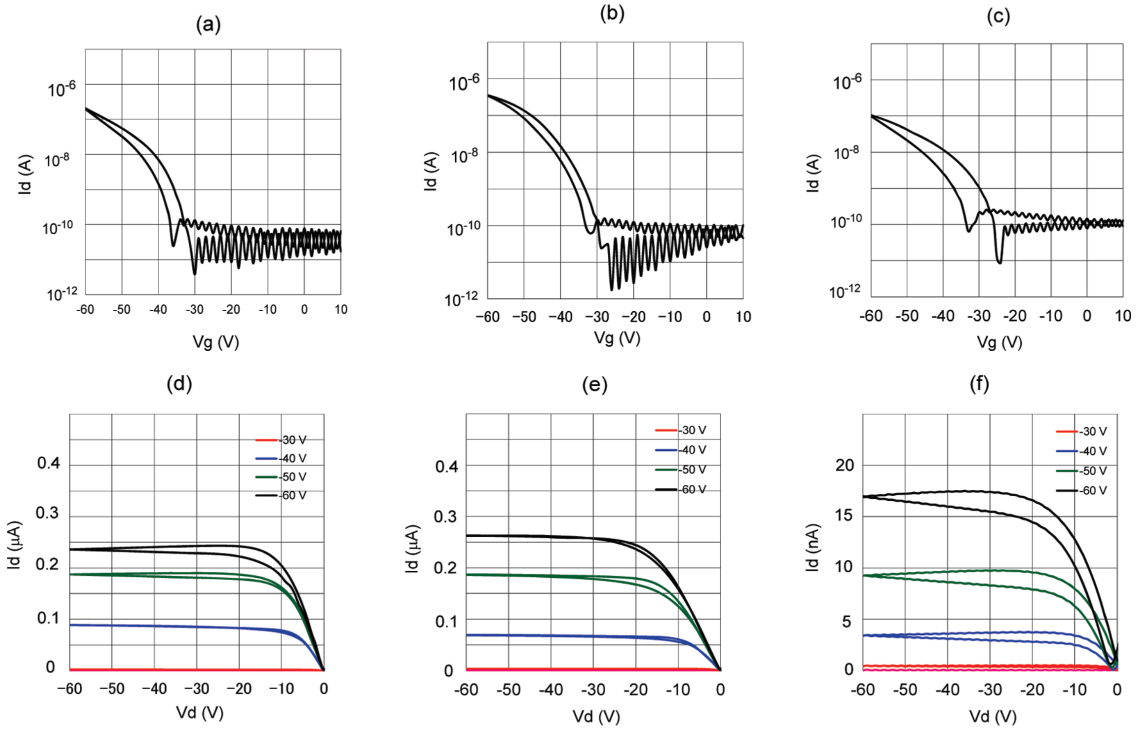

Figure 8. Transfer characteristics at −60 V drain voltage (top) and output curves at different gate voltages (bottom) of FETs based on **1** and **2**. (a) and (d): FET of 1 after ODTS treatment and annealing (entry 2 in Table 4), (b) and (e): FET of 1 with longer source/drain pair after ODTS treatment and annealing (entry 3 in Table 4), (c) and (f): FET of 2 after annealing (entry 5 in Table 4).

was available from TCI. Pd/C (10%) was obtained from Wako Pure Chemical Co. Tributyl(5-phenyl-2-thienyl)tin was prepared from 2-phenylthiophene and tributyltin chloride according to the literature.[15]

Synthesis of 1. 3,7-Dibromobenzodithiophene **10** (200 mg, 0.29 mmol) (see Scheme 1 and the Supporting Information for the preparation), tributyl(5-phenyl-2-thienyl)tin (300 mg, 0.67 mmol), $Pd(PPh_3)_4$ (24 mg, 0.020 mmol), DMF (3 mdm^3), and toluene (3 mdm^3) were placed in a 20 mdm^3 two-necked reaction flask. The solution was stirred at 85 °C for 24 h. The mixture was quenched with water, extracted with toluene, and evaporated in vacuo. The residue was purified by column chromatography with toluene followed by washing with acetone afforded the X-shaped oligomer, 3,7-didocecyl-2,6-di(5-phenylthiophen-2-yl)benzo[1,2-*b*:3,4-*b*′]dithiophene (**1**, 200 mg, 0.23 mmol) in 81% yield as a yellow solid. ^1H NMR (400 MHz, $CDCl_3$) δ 7.68−7.62 (m, 6H), 7.45−7.37 (m, 4H), 7.44−7.34 (m, 4H), 7.26−7.23 (m, 2H), 3.10 (t, *J* = 7.6 Hz, 4H), 1.81−1.70 (m, 4H), 1.55−1.45 (m, 4H), 1.42−1.20 (m, 32H), 0.88 (t, *J* = 6.8 Hz, 6H); ^{13}C NMR (100 MHz, $CDCl_3$) δ 145.2, 138.7, 135.8, 134.7, 134.3, 132.2, 129.8, 129.2, 128.0 (2C), 126.0, 123.7, 119.3, 32.2, 30.4, 30.1, 29.93 (2C), 29.89, 29.88, 29.69, 29.59, 28.1, 22.9, 14.3; HRMS (EI): *m*/*z* (M^+) calcd for $C_{54}H_{66}S_4$: 842.4047, found: 842.4055.

Synthesis of 2. Using 2,6-dibromo-4,7-didodecylbenzo[1,2-*b*:3,4-*b*′]dithiophene (**11**, 270 mg, 0.39 mmol), which was prepared according to the literature,[4] as the starting material, the coupling with tributyl(5-phenyl-2-thienyl)tin (420 mg, 0.94 mmol) was carried out under the same palladium catalysis as described in the synthesis of **1**. The cross-shaped oligomer, 4,8-didocecyl-2,6-di(5-phenylthiophen-2-yl)benzo[1,2-*b*:3,4-*b*′]dithiophene (**2**, 240 mg, 0.28 mmol, 73%) was isolated as an orange solid. ^1H NMR (400 MHz, $CDCl_3$) δ 7.66−7.58 (m, 4H), 7.48 (s, 2H), 7.44−7.34 (m, 4H), 7.33−7.26 (m, 6H), 3.11 (t, *J* = 7.6 Hz, 4H), 1.88−1.78 (m, 4H), 1.55−1.45 (m, 4H), 1.42−1.20 (m, 32H), 0.86 (t, *J* = 6.4 Hz, 6H); ^{13}C NMR (100 MHz, $CDCl_3$) δ 144.5, 137.4, 137.3, 137.1, 136.6, 134.2, 129.2, 128.8, 128.0, 126.1, 125.9, 124.1, 117.9, 33.6, 32.2, 30.2, 29.96 (2C), 29.90, 29.84, 29.77 (2C), 29.59, 22.9, 14.3; HRMS (EI): *m*/*z* (M^+) calcd for $C_{54}H_{66}S_4$: 842.4047, found: 842.4061.

Flash-Photolysis Time Resolved Microwave Conductivity (FP-TRMC) Mearsurement. The nanosecond laser pulses from a Nd: YAG laser (third harmonic generation, THG (355 nm) from Spectra Physics, INDY-HG (fwhm 5−8 ns) have been used as excitation sources. The power density of the laser was set at 5.2 × 10^{14} to 8.9 × 10^{16} photons cm^{-2}. For time-resolved microwave conductivity (TRMC) measurement, the microwave frequency and power were set at ∼9.1 GHz and 3 mW respectively. The TRMC signal picked up by a diode (rise time <1 ns) is monitored by a digital oscilloscope of Tektronix TDS3032B. All the above experiments were carried out at room temperature. The transient photoconductivity of the samples is propotional to the reflected microwave power (ΔPr/Pr) and sum of the mobilities of charge carriers via:

$$\frac{1}{A}\frac{\Delta P_r}{P_r} = e\varphi N\sum\mu \qquad (1)$$

where *A*, *e*, *φ*, *N*, and $\sum\mu$ are a sensitivity factor, elementary charge of electron, photo carrier generation yield (quantum efficiency), the number of absorbed photons per unit volume, and sum of mobilities for negative and positive carriers, respectively. Polarization of the laser pulses is isotropic.

The compounds were dissolved in *o*-dichlorobenzene and cast onto quartz substrate at 0.6−2.1 μm thick determined by Dektak150 surface profiler. The films were heated up to 200 °C under an Ar atmosphere and annealed at the temperature for 30 min before the measurement. The number of photons absorbed by the film is estimated by the direct measurement of transmitted power of laser pulses Opher NOVA-display power meter.

Time-of-Flight Mearsurement. The compounds **1** and **2** were overcoated onto an Al electrode from *o*-dichlorobenzene solutions at 8.0 and 4.2 μm thick, respectively. The films were annealed at 200 °C for 3 h under high vacuum. The film was subsequently overcoated by an Au semitransparent electrode. The measurement was carried out in an environmental chamber at 273 K, > 10^{-4} Pa. The nanosecond laser pulses from a Nd: YAG laser (third harmonic generation, THG (355 nm) from Spectra Physics, Quanta-Ray (fwhm 5−8 ns) have been used as excitation sources. The power density of the laser was set at 2.0 × 10^{15} photons cm^{-2}. Current transients were recorded through a terminate resistance of 3 kΩ by a Tektronic TDS 3052B digitizing oscilloscope. The bias voltage was applied to the top electrode by an ADVANTEST R8252 power source. Photogenerated charge carriers are estimated by an integration of the current transient, with simultaneous accumulation by a Keithley R6487 current integrator. The other set of apparatus is described in elsewhere.[16]

FET Measurement. FET devices based on **1** and **2** as the semiconductors were fabricated with top contact configuration on silicon wafer in inert conditions. A heavily n-doped silicon wafer with a 300-nm thermal silicon dioxide (SiO_2) was used as the substrate/gate electrode, with the top SiO_2 layer serving as the gate dielectric. Two types of wafer were prepared; one was employed without any special pretreatments and the other was immersed in a solution of octadecyltrichlorosilane (ODTS, 200 $\mu\mathrm{dm}^3$) in octane (50 mdm^3) overnight prior to fabrication. The active layers were deposited on top of SiO_2 surface by spin-coating a solution of **1** or **2** in toluene (0.5 wt %). Subsequently, some wafers were annealed at 60 °C for 30 min. MoO_3 (15 nm) and Au (50 nm) were sequentially deposited by vacuum evaporation through a shadow mask to create a source/drain pair. The channel width (W) and length (L) were 2000 μm and 20 (or 50) μm, respectively. The field-effect mobility (μ) was calculated in the saturation region at the V_d of −60 V using the following equation: $I_d = \mu C_i(V_g - V_{th})^2$, where C_i is the capacitance of SiO_2, and V_g and V_{th} are gate voltage and threshold voltage, respectively.

■ ASSOCIATED CONTENT

Ⓢ Supporting Information. Preparation of compound **10**, detailed characterization data of compounds **6**−**11**, and XRD patterns of some devices based on **1** and **2**. This material is available free of charge via the Internet at http://pubs.acs.org.

■ AUTHOR INFORMATION

Corresponding Author

*E-mail: seki@chem.eng.osaka-u.ac.jp; miura@chem.eng.osaka-u.ac.jp.

■ ACKNOWLEDGMENT

This work was supported, in part, by Grants-in-Aid from the Ministry of Education, Culture, Sports, Science, and Technology, Japan, and by the cooperative research with Sumitomo Chemical Co., Ltd.

■ REFERENCES

(1) Recent reviews:(a) Katz, H. E.; Bao, Z.; Gilat, S. L. *Acc. Chem. Res.* **2001**, *34*, 359. (b) Takimiya, K.; Kunugi, Y.; Otsubo, T. *Chem. Lett.* **2007**, *36*, 578. (c) Murphy, A. R.; Fréchet, J. M. J. *Chem. Rev.* **2007**, *107*, 1066. (d) Ong, B. S.; Wu, Y.; Li, Y.; Liu, P.; Pan, H. *Chem.—Eur. J.* **2008**, *14*, 4766. (e) Allard, S.; Forster, M.; Souharce, B.; Thiem, H.; Schert, U. *Angew. Chem., Int. Ed.* **2008**, *120*, 4138. (f) Chen, J.; Cao, A. Y. *Acc. Chem. Res.* **2009**, *42*, 1709.

(2) For a recent example of β,β'-dialkylthiophene derivatives with high charge carrier mobility and conductivity:(a) Prasanthkumar, S.; Saeki, A.; Seki, S.; Ajyayaghosh, A. *J. Am. Chem. Soc.* **2010**, *132*, 8866. (b) Prasanthkumar, S.; Gopal, A.; Ajayaghosh, A. *J. Am. Chem. Soc.* **2010**, *132*, 13206.

(3) (a) Pan, H.; Li, Y.; Wu, Y.; Liu, P.; Ong, B. S.; Zhu, S.; Xu, G. *Chem. Mater.* **2006**, *18*, 3237. (b) Pan, H.; Wu, Y.; Li, Y.; Liu, P.; Ong, B. S.; Zhu, S.; Xu, G. *Adv. Funct. Mater.* **2007**, *17*, 3574.

(4) Pan, H.; Li, Y.; Wu, Y.; Liu, P.; Ong, B. S.; Zhu, S.; Xu, G. *J. Am. Chem. Soc.* **2007**, *129*, 4112.

(5) (a) Higa, T.; Krubsack, A. J. *J. Org. Chem.* **1975**, *40*, 3037. (b) Ried, W.; Oremek, G.; Ocakcioglu, B. *Liebigs Ann. Chem.* **1980**, 1424. (c) Malešević, M.; Karminsky-Zamola, G.; Bajić, M.; Boykin, D. W. *Heterocycles* **1995**, *41*, 2691.

(6) Gelman, D.; Buchwald, S. L. *Angew. Chem., Int. Ed.* **2003**, *42*, 5993.

(7) (a) Yamamoto, T.; Komarudin, D.; Arai, M.; Lee, B. L.; Suganuma, H.; Asakawa, N.; Inoue, Y.; Kubota, K.; Sasaki, S.; Fukuda, T.; Matsuda, H. *J. Am. Chem. Soc.* **1998**, *120*, 2047. (b) Ong, B. S.; Wu, Y.; Liu, P.; Gardner, S. *J. Am. Chem. Soc.* **2004**, *126*, 3378. (c) Wu, Y.; Liu, P.; Gardner, S.; Ong, B. S. *Chem. Mater.* **2005**, *17*, 221.

(8) Frisch, M. J.; Trucks, G. W.; Schlegel, H. B.; Scuseria, G. E.; Robb, M. A.; Cheeseman, J. R.; Montgomery, Jr., J. A.; Vreven, T.; Kudin, K. N.; Burant, J. C.; Millam, J. M.; Iyengar, S. S.; Tomasi, J.; Barone, V.; Mennucci, B.; Cossi, M.; Scalmani, G.; Rega, N.; Petersson, G. A.; Nakatsuji, H.; Hada, M.; Ehara, M.; Toyota, K.; Fukuda, R.; Hasegawa, J.; Ishida, M.; Nakajima, T.; Honda, Y.; Kitao, O.; Nakai, H.; Klene, M.; Li, X.; Knox, J. E.; Hratchian, H. P.; Cross, J. B.; Bakken, V.; Adamo, C.; Jaramillo, J.; Gomperts, R.; Stratmann, R. E.; Yazyev, O.; Austin, A. J.; Cammi, R.; Pomelli, C.; Ochterski, J. W.; Ayala, P. Y.; Morokuma, K.; Voth, G. A.; Salvador, P.; Dannenberg, J. J.; Zakrzewski, V. G.; Dapprich, S.; Daniels, A. D.; Strain, M. C.; Farkas, O.; Malick, D. K.; Rabuck, A. D.; Raghavachari, K.; Foresman, J. B.; Ortiz, J. V.; Cui, Q.; Baboul, A. G.; Clifford, S.; Cioslowski, J.; Stefanov, B. B.; Liu, G.; Liashenko, A.; Piskorz, P.; Komaromi, I.; Martin, R. L.; Fox, D. J.; Keith, T.; Al-Laham, M. A.; Peng, C. Y.; Nanayakkara, A.; Challacombe, M.; Gill, P. M. W.; Johnson, B.; Chen, W.; Wong, M. W.; Gonzalez, C.; and Pople, J. A. *Gaussian 03*; Gaussian, Inc., Wallingford CT, 2004.

(9) Saeki, A.; Seki, S.; Tagawa, S. *J. Appl. Phys.* **2006**, *100*, 023703.

(10) Microwave measurement of mobility with ESR method: Marumoto, K.; Arai, N.; Goto, H.; Kijima, M.; Murakami, K.; Tominari, Y.; Takeya, J.; Shimoi, Y.; Tanaka, H.; Kuroda, S.; Kaji, T.; Nishikawa, T.; Takenobu, T.; Iwasa, Y. *Phys. Rev. B* **2011**, *83*, 075302–1.

(11) Funston, A. M.; Silverman, E. E.; Miller, J. R.; Schanze, K. S. *J. Phys. Chem. B* **2004**, *108*, 1544.

(12) (a) Levin, E. I.; Shklovskii, B. I. *Solid State Commun.* **1988**, *67*, 233. (b) Kunimi, Y.; Seki, S.; Tagawa, S. *Solid State Commun.* **2000**, *114*, 469.

(13) See Supporting Information for our preliminary studies on the molecular orientation and intermolecular interaction by the X-ray diffraction (XRD) measurements.

(14) (a) Umeda, N.; Tsurugi, H.; Satoh, T.; Miura, M. *Angew. Chem., Int. Ed.* **2008**, *47*, 4019. (b) Horita, A.; Tsurugi, H.; Funayama, A.; Satoh, T.; Miura, M. *Org. Lett.* **2007**, *9*, 2231.

(15) Pelter, A.; Jenkins, I.; Jones, D. E. *Tetrahedron* **1997**, *53*, 10357.

(16) (a) Seki, S.; Yoshida, Y.; Tagawa, S.; Asai, K.; Ishigure, K.; Furukawa, K.; Fujiki, M.; Matsumoto, N. *Phil. Mag. B* **1999**, *79*, 1631. (b) Acharya, A.; Seki, S.; Koizumi, Y.; Saeki, A.; Tagawa, S. *J. Phys. Chem. B* **2005**, *109*, 20174.